A novel 1,3,5-triaminocyclohexane-based tripodal ligand forms a unique tetra(pyrazolate)-bridged tricopper(II) core: solution equilibrium, structure and catecholase activity†

Attila Szorcsik[a], Ferenc Matyuska[b], Attila Bényei[c], Nóra V. Nagy[d], Róbert K. Szilágyi[e] and Tamás Gajda[a,b,*]

Abstract

Copper(II) complexes of a polydentate tripodal ligand **L**×3HCl (**L** = N,N',N''-tris(5-pyrazolylmethyl)-*cis,cis*-1,3,5-triaminocyclohexane) were characterized in both solution and solid states. Combined evaluation of potentiometric, UV-VIS, and EPR data indicated the formation of two mononuclear (CuH**L**, Cu**L**) and three trinuclear ($Cu_3H_{-x}\mathbf{L}_2$, x = 2, 3, 4) complexes. The triply deprotonated trinuclear complex is an efficient catechol oxidase mimic with a surprisingly low pH optimum at pH = 5.6. Since the mononuclear Cu**L** species is not able to promote the oxidation of 3,5-di-tert-butylcatechol, we assume that the central copper(II) ion of the trinuclear complex with unsaturated coordination sphere has fundamental role in the binding and oxidation of the substrate.

The high stability and spectroscopic properties of the Cu**L** species indicate the coordination of two pyrazole rings in addition to the three secondary amino groups of **L** in a square pyramidal geometry. Parallel with the formation of trinuclear species, intense charge transfer bands appear at around 400–500 nm, which indicate the formation of pyrazolate-bridged complexes. The crystal structure of $[Cu_3H_{-4}\mathbf{L}_2](ClO_4)_2\times5H_2O$ (**1**) reveals the formation of a unique trinuclear complex that features a tetra(pyrazolate)-bridged linear tricopper(II) core. The Cu···Cu interatomic distances are around 3.8 Å. The two peripheral copper(II) ions have slightly distorted square pyramidal geometry. The four pyrazole rings bound to the peripheral copper(II) ions are deprotonated that create a flattened tetrahedral environment for the central copper(II), *i.e.* the formation of the trinuclear complexes is under the allosteric control of the two peripheral copper(II) ions. The experimental structural details were further elaborated by a series of hybrid density functional theory calculations that support the presence of an antiferromagnetically coupled ground state. However, the magnitude and the pattern of spin coupling are dependent on the composition of the functionals. The optimized theoretical structures highlight the role of the crystal packing effects in inducing asymmetry between the two peripheral copper(II) sites.

[a] *MTA-SZTE Bioinorganic Chemistry Research Group, Dóm tér 7, H-6720 Szeged, Hungary*
[b] *Department of Inorganic and Analytical Chemistry, University of Szeged, Dóm tér 7, H-6720 Szeged, Hungary. E-mail: gajda@chem.u-szeged.hu*
[c] *Department of Pharmaceutical Chemistry, University of Debrecen, Egyetem tér 1, Debrecen H-4032, Hungary*
[d] *Institute of Organic Chemistry, Research Centre for Natural Sciences HAS, Magyar tudósok körútja 2, H-1117 Budapest, Hungary*
[e] *Department of Chemistry and Biochemistry, Montana State University, Bozeman, MT 59717 USA and Department of Analytical Chemistry, Faculty of Engineering, University of Pannonia, Veszprém, 8201, Hungary*

† **Electronic supplementary information available**: ESI-MS and ^{1}H NMR spectra of the ligand, crystallographic data, figures of the stereogenic centers and packing diagram of the unit cell, XYZ coordinates of optimized structures, summary of calculated geometric structures as a function of HF content in hybrid density functional, single-crystal EPR, UV-VIS spectra and cyclic voltammogramm of the trinuclear. See DOI : ???. Computational results, ionic fragments, and checkpoint files with converged electronic structures can be downloaded at computational.chemistry.montana.edu/SI.

Introduction

Oligonuclear metallocenters are widespread in metalloenzymes, since the metal ions may act cooperatively to accomplish a given chemical function. Some of the functional models designed to mimic the oligonuclear motif of metalloenzymes were demonstrated to be far more active than their mononuclear counterparts.[1-3] We also developed a few highly active binuclear enzyme mimics.[4-11] On the other hand, a great number of low molecular weight enzyme models studied also emphasized the importance of the adequate and preorganized structure around the metal ions, which is trivially present in enzymes. Although a large number of metal complexes formed with linear/acyclic ligands were reported to possess important catalytic activity,[4-6,12,13] tripodal compounds may have several advantages over the linear ones, such as the preorganized structure, higher metal binding ability and facial coordination.[14] Tripodal ligands, such as *cis,cis*-1,3,5-triaminocyclohexane (tach) and related compounds (1,3,5-triamino-1,3,5-trideoxy-*cis*-inositol (taci) and its N-methylated derivatives), are versatile ligands with several unique coordination properties.[15] We and others demonstrated the important hydrolytic activity of their copper(II) complexes towards both amide[16] and phosphodiester bonds.[8-11,17-19].

Hexadentate ligands obtained by N-substitution of tach draw considerable attention due to their ideal donor sets for metal ion coordination. The [3N3O] donor set of *cis,cis*-1,3,5-tris{(2-hydroxybenzyl)aminomethyl}cyclohexane forms highly stable lipophilic complexes with M(III) metal ions,[20,21] and the substitution of the benzyl-ring provided a series of Mn-SOD models with tunable reduction potentials.[22] Tachpyr (N,N',N''-tris(2-pyridylmethyl)-*cis,cis*-1,3,5-triaminocyclohexane) and its close derivatives form also very stable [6N] complexes with a range of transition metal ions.[23-25] It is worth nothing that the cytotoxicity of tachpyr is probably related to its significant metal ion binding ability.[26]

Derivatization of the legs of tripodal platforms provides additional donor site(s), may influence the steric environment around the metal center, as well as may help to introduce additional functions, such as substrate binding or activation. The preorganization of the tripodal scaffold can be substantially increased by allosteric metal ion(s), which may create high affinity binding site(s) for the catalytic metal ion(s). In order to develop such an oligonuclear core by allosteric interaction, the N-substituted tach ligand needs to accommodate additional metal binding site(s), for which purpose pyrazole-substituted tach derivarives are appropriate candidates. Pyrazolate-bridged metal complexes have received significant attention over recent decades, among others, due to their unique ability to self-assemble into supramolecular architectures. Pyrazolate moieties are well suited to position

two metal ions in close proximity,[27,28] and such centers may efficiently mimic the function of both hydrolase[29] and oxidoreductase enzymes.[30]

Our aim was to explore the combined advantages of the preorganized structure of tripodal scaffolds and the metal bridging ability of pyrazole rings in order to develop a new oligometallic core under allosteric control, which may potentially mimic the function of oxidase enzymes. Accordingly, we synthetized the ligand N,N',N''-tris(5-pyrazolylmethyl)-1,3,5-*cis,cis*-triamino-cyclohexane (**L**, tachpyz) and studied its complexes formed with copper(II) both in solution and in solid state. Spectroscopically calibrated, hybrid DFT calculations were used to gain deeper insights into the electronic structure and spin-coupling scheme by considering both ferro- and antiferromagnetic ground states. To screen the enzyme mimetic properties of the copper(II) complexes their catecholase activity was studied by using 3,5-di-tert-butylcatechol (H_2dtbc) as model substrate.

Materials and methods

Materials

All reagents were of analytical grade and used without further purification. Copper(II) perchlorate solution were prepared from analytically pure compounds obtained from Sigma-Aldrich and standardized complexometrically. A 0.1 M NaOH standard solution (Sigma) was used for pH titrations. The compound 1-H-pyrazole-5-carboxaldehyde (97%) was purchased from Novo Chemy Ltd. The buffers MES 2-([N-morpholino]ethanesulfonic acid (MES), N-(2-hydroxyethyl)piperazine-N'-ethanesulfonic acid (HEPES) and 2-(cyclohexylamino)-ethanesulfonic acid (CHES) were purchased from Sigma-Aldrich. Tach×3HBr was prepared as reported in the literature.[31]

Synthesis of N,N',N''-tris(5-pyrazolylmethyl)-1,3,5-cis,cis-triamino-cyclohexane×3HCl (tachpyz, L×3HCl)

Tach×3HBr (1.008 g, 2.708 mmol) was dissolved in H_2O (4 mL) with NaOH (0.325 g, 8.125 mmol) to form a clear solution. Benzene (70 mL) was added and the water was removed by azeotropic distillation using a Dean-Stark trap. After cooling, the solution was rotary evaporated to a white solid. The residue was dissolved in MeOH (50 mL) and 1-H-pyrazole-5-carboxaldehyde (0.7808 g, 8.1 mmol) was added. The mixture was refluxed 8 hr. After cooling the solution, $NaBH_4$ (0.68 g, 17 mmol) was added to reduce the Schiff-base formed.

The solution was stirred for 24 hr after which the solvent was removed by rotary evaporation. The residue was taken up in EtOH (30 mL) and the pH was set to 2 with concentrated HCl to precipitate the boric acid derivatives. After filtering, the filtrate was treated with dry HCl gas, which resulted in precipitation of the pure **L**×3HCl (Scheme 1). The product was washed with dry EtOH (50 mL) and dry Et_2O (50 mL). Yield 1.11 g (86%). The purity was checked by ^{1}H-NMR in 10%-90% D_2O/H_2O at pH = 3.5 (7.71, d, 3H (J = 2.3 Hz); 6.45, d, 3H (J = 2.3 Hz); 4.33, s, 6H; 3.40, tt, 3H (J = 12 and 3.6 Hz); 2.95, dt, 3H (J = 12 and 3.6 Hz); 1.69, dt, 3H (J = 12 and 12 Hz), no other signals were detected, see Fig. S1 in Electronic Supporting Information). (HR)ESI-MS m/z = 370.2467, calculated for $C_{18}H_{27}N_9$ $[M+H]^+$ = 370.2468 (see Fig. S2 in ESI).

X-ray Data Collection and Crystal Structure Determinations

Crystallographic and experimental details of the data collection and refinement of the structure of $[Cu_3H_{-4}\mathbf{L}_2](ClO_4)_2\times5H_2O$ (**1**) are reported in Table 1. The brown complex **1** was crystallized by slow evaporation from water containing copper(II) and tachpyz in a 1.4/1 ratio at pH 8.0 standing at room temperature for about 1 week. Several batches of crystals were studied by single crystal X-ray diffraction method. XRD data collection was carried out at 293 K using Mo-Kα radiation (λ = 0.71073 Å) with a Burker-Nonius MACH3 diffractometer equipped with point detector. Unexpectedly, the crystals diffracted rather poorly that resulted only small intensity peaks with a point detector. Several datasets were collected and merged. However, as the quality of the structure determination was still low, new datasets were collected using an Agilent SuperNova diffractometer equipped with a CCD detector at 100 K using Cu-Kα radiation (λ = 1.54184 Å). The structure was solved by SIR-92 program[32] and refined by full-matrix least-squares method on F^2. Non-hydrogen atoms were refined with anisotropic thermal parameters using the SHELX package.[33] Disorder of the perchlorate ion could be modelled but orientation of some of the water molecules remained ambiguous resulting checkcif errors but this does not influence the overall structure determination of the complex and only the hydrogen bond web remained somewhat uncertain. Altogether five solvent water molecules were found and one of them is distributed among two places with equal occupancy of 0.5. The hydrogen atoms of these disordered water molecule could not be located. Alternative atom type assignments in the non-bound C11-C15 and C61-C65 pyrazole rings are possible, *i.e* N12 and N13 can be replaced with C15 and C14 and similarly N62 and N63 can be replaced with C65 and C64, and location of the pyrazole protons are also tentative. Publication material was prepared with the WINGX-suite.[34] Hydrogen atoms were

treated with a mixture of independent and constrained refinement. Hydrogens of the methylene and amine groups, as well as aromatic hydrogens were placed according to ideal geometric position. Hydrogen atoms of water molecules were found at the difference electron density map but the distances of hydrogen and oxygen atoms were restrained in the final stage of the refinement. All crystallographic data are deposited in the Cambridge Crystallographic Data Centre under CCDC 1410354.

Potentiometric Measurements

The protonation and coordination equilibria were investigated by potentiometric titrations in aqueous solution (I = 0.1 M NaCl, and T = 298.0 ± 0.1 K) under Ar using an automatic titration set including a PC controlled Dosimat 665 (Metrohm) autoburette and an Orion 710A precision digital pH-meter. The Metrohm Micro pH glass electrode (125 mm) was calibrated[35] *via* the modified Nernst equation (1):

$$E = E_0 + K \cdot \log[\mathrm{H}^+] + J_{\mathrm{H}} \cdot [\mathrm{H}^+] + \frac{J_{\mathrm{OH}} \cdot K_{\mathrm{w}}}{[\mathrm{H}^+]} \quad (1)$$

where J_{H} and J_{OH} are fitting parameters in acidic and alkaline media for the correction of experimental errors, mainly due to the liquid junction and to the alkaline and acidic errors of the glass electrode; $K_{\mathrm{w}} = 10^{-13.75}$ M^2 is the auto-ionization constant of water.[36] The parameters were calculated by the non-linear least squares method. The complex formation was described by a general equilibrium process as follows:

$$\mathrm{pM} + \mathrm{qH} + \mathrm{rL} \xleftrightarrow{\beta_{\mathrm{M_pH_qL_r}}} \mathrm{M_pH_qL_r} \quad (2)$$

$$\beta_{\mathrm{M_pH_qL_r}} = \frac{[\mathrm{M_pH_qL_r}]}{[\mathrm{M}]^{\mathrm{p}}[\mathrm{H}]^{\mathrm{q}}[\mathrm{L}]^{\mathrm{r}}} \quad (3)$$

where M denotes the metal ion, L the non-protonated ligand molecule, and H stands for protons. Charges are omitted for simplicity, but can be easily calculated taking into account that the composition and charge of the ligand at pH 2 is $\mathrm{H_3L}^{3+}$. The corresponding formation constants ($\beta_{\mathrm{M_pH_qL_r}} \equiv \beta_{\mathrm{pqr}}$) were calculated using the PSEQUAD computer program.[37]

The protonation constants were determined from four independent titrations (90 data points per titration), with ligand concentration 2–3×10^{-3} M. The complex formation constants were evaluated from seven independent titrations (~90 data points per titration). The metal-to-ligand ratios were 2:1, 3:2, 1:1, and 1:2. At 2:1 and 3:2 ratios precipitate was observed above pH 6 and 9, respectively. Therefore, the data collected above these pH were not used in our

calculations. The metal ion concentrations varied between 1.0–2.9×10^{-3} M, depending on the metal-to-ligand ratio. The titrations were performed between pH 1.9 and 11.4.

Electronic Absorption and CV Measurement

UV-Vis spectra were measured on Unicam Helios α or Thermo Scientific Evolution 200 spectrophotometers using a cell with 1 cm optical pathlength. Similar concentrations were used as described above for the potentiometric titrations. The individual UV-Vis spectra of the complexes were calculated by PSEQUAD.[37] Cyclic voltammetry measurements were performed on a conventional three-electrode system in Ar atmosphere and a PC controlled Electrochemical Measurement System (EF 451) at 100 mV s^{-1} scan rate and in the range of −1.2 V to +1.5 V. A glassy carbon electrode was used as the working electrode, a platinum electrode as the auxiliary electrode, and Ag/AgCl/KCl (1 M) as reference electrode. Electrochemical potentials were converted into the normal hydrogen electrode (NHE) scale by adding 0.236 V. The electrochemical system was calibrated with aqueous solution of 1 mM ferrocene (0.1 M NaCl). Cyclic voltammograms of the copper(II) complexes were determined at 25.0 ± 0.1 °C in 50% (v/v) ethanol-water solution (0.1 M NaCl) containing 2.9×10^{-3} M metal ion and 2×10^{-3} M ligand.

EPR and NMR Measurements

The EPR spectra were recorded at room temperature and at 77 K using a BRUKER EleXsys E500 spectrometer (microwave frequency 9.81 GHz, microwave power 13 mW, modulation amplitude 5 G, modulation frequency 100 kHz). The EPR spectra were determined in aqueous solutions (with the exception of the single crystal sample, see Figure S6), and were simulated by a spectral decomposition algorithm.[38] Since the copper(II) salt used to make the stock solution was a natural mixture of isotopes, the spectrum of each species was calculated as the sum of spectra containing ^{63}Cu and ^{65}Cu weighted by their natural abundances. The copper and ligand coupling constants are given in units of gauss (1 G = 10^{-4} T).

The ^{1}H NMR measurements were performed on a Bruker Avance DRX 500 spectrometer. The spectra were recorded at 25 °C in 100% D_2O solution, at a tachpyz concentration of 3.0×10^{-3} M with a tube diameter of 5 mm. The chemical shifts (δ) were measured relative to dioxane as internal reference and converted to $SiMe_4$ reference using $\delta_{dioxane}$ = 3.70. Data were processed using the Topspin 2.0 software package (Bruker).

Determination of the Catechol Oxidase Activity

The 2-electron oxidation of 3,5-di-*tert*-butylcatechol (H_2dtbc, Scheme 2) in the presence and absence of the copper(II)-tachpyz system was monitored spectrophotometrically on a Unicam Helios α spectrophotometer by following the increase of the 3,5-di-*tert*-butyl-o-benzoquinone (dtbq) absorption band at 406 nm (ε = 1900 M^{-1} cm^{-1}). Due to the low solubility of dtbq in water, our experiments were performed in O_2-saturated 50% (m/m) ethanol-water mixture. The mixture of dioxygen- and argon saturated solutions were used to determine the dependence of the rate on the dioxygen concentration. For the determination of the pH in this mixed solvent, the glass electrode was calibrated by standard aqueous buffer solutions at pH = 4.0, 7.0, and 10. The actual pH was calculated by subtracting 0.21 units from the pH-meter reading according to the method of Bates.[39] A pK_w value of 14.84 was used for the auto-ionization constants of water in 50% (m/m) ethanol-water.[40] The auto-oxidation of 3,5-di-*tert*-butylcatechol was also determined for each substrate concentration and pH value to be subtracted from the overall effect in order to obtain the extent of the oxidation solely catalyzed by copper(II)-tachpyr complexes. Kinetic studies were carried out by the method of initial rates (if the reaction was sufficiently fast, the data between 2-5 % conversion was used), but in some cases the integral method (up to 90% conversion) was used. The reported data are averages of three parallel experiments. The maximum deviation from the main value did not exceed 10 %.

Density Functional Theory Modelling of Geometric and Electronic Structures

Given the sensitivity of the electronic structure of copper(II) complexes with respect of the composition of density functionals and the quality of the basis set employed,[41] we evaluated the electronic structure of the copper(II)-tachpyz system using a range of hybrid GGA functionals. These included pure DFT functionals of BP86,[42] the commonly used B3LYP[43] hybrid functionals, and systematically varied composition with 18%, 38%, 75%, 100% HFX and Becke88 exchange[42a] with Perdew86 correlation[42b] functionals. The hybrid functional B(38HF)P86 was already shown to be spectroscopically calibrated for a series of copper(II) containing bioinorganic complexes and metalloprotein active sites.[44] A hybrid functional with 18% HF exchange was chosen to evaluate the effect of correlation functionals between B(18HF)P86 and B3LYP functionals. The basis set employed (def2TZVP[45]) is larger than needed for the saturation limit as defined earlier.[44,46]

The desired spin coupling scheme among the three copper(II) sites in $[Cu_3H_{-4}L_2]^{2+}$ complex was achieved by using the generalized ionic fragment approach (GIFA[47]). First, the well

defined electronic structures of the copper(II) ion and the deprotonated tachpyz ligand were generated at the HF level. The relaxed electronic structures of these fragments were merged into to an initial guess of molecular orbital for the $[Cu_3H_{-4}L_2]$ complex, as an ionic limit for the electronic structure without covalent interactions. This was sequentially relaxed in a more and more covalent calculation as the amount of HF exchange was decreased from 100% to 0% and in parallel the DF exchange was increased from 0% to 100% at the pure GGA level.

Results and Discussions

Crystal structure of $[Cu_3H_{-4}L_2](ClO_4)_2\times5H_2O$ (1)

The brown complex **1** was crystallized by slow evaporation from water containing copper(II) and tachpyz in a 1.4/1 ratio at pH 8.0 standing at room temperature for about 1 week. A representative set of bond lengths, interatomic distances, and bond angles of **1** are listed in Table 2 (the full list of data are collected in Table S2, see ESI). Figure 1 shows a PLUTO representation of **1** including partial numbering scheme. The crystal structure confirms the existence of a unique trinuclear complex that features a tetra(pyrazolato) bridged linear tricopper(II) arrangement. The peripheral Cu1– central Cu2 and central Cu2– peripheral Cu3 interatomic distances are 3.773 Å and 3.828 Å, respectively. The two peripheral copper(II) ions have a slightly distorted square pyramidal geometry (τ = 0.093 (Cu1) and 0.070 (Cu3)).[48] Their basal planes are formed by two secondary amino groups and two pyrazolato nitrogens. The copper(II)-nitrogen bond lengths fall in the range of 1.931-1.973 and 2.031-2.262 Å for the pyrazolato and secondary amino nitrogens, respectively. As expected, the Cu-N bond lengths of the apically bound third secondary amino nitrogens are more elongated (2.219(4) and 2.262(4) Å for Cu1 and Cu3 sites, respectively). The four deprotonated pyrazole rings bound to the peripheral copper(II) ions create a tetrahedral environment for the central Cu2, resulting in the formation of four pyrazolate bridges. The average central Cu2-N distance is 1.967 Å. The tetrahedron around Cu2 is considerably flattened as the bond angles around central Cu2 are between 95.7(2)° and 136.5(2)°, while the angle between the N21-Cu2-N31 and N71-Cu2-N81 chelate planes is ω = 61.2°. The distortion of the tetrahedral geometry towards square planar is facilitated by the steric hindrance of the two *bis*-bidentate pyrazolate chelates, and the Jahn-Teller distortion force due to the $3d^9$ electron configuration of copper(II) ion. Search of the Cambridge Structural Database[49] (version 5.36 update May, 2015) revealed no similar trinuclear pyrazolate-bridged copper(II) complex. Expanding the search for other metal ions the tetra(pyrazolato) bridged trinuclear mixed-valent complex $[Co^{III}(L')Co^{II}(L')Co^{III}(Cl)_4]$ (where H_2L' = 1,3-bis(3-methyl-5-formylpyrazolylmethinimino)-propane-2-ol) has the sole similar structure, where the C3 carbons of the pyrazolato bridges are methyl-substituted, therefore the tetrahedron around the central cobalt(II) is only slightly flattened (ω = 84°).[50]

Complex **1** was prepared using non-chiral reagents and the racemate crystallized in the centrosymmetric space group (P21/c, No. 14) as expected. However, the stereogenic centers in the Cu1-coordinating ligand (N1, N2, N3, C3 and C5) and the corresponding stereogenic

centers in the Cu3-coordinating ligand have opposite configuration (see Figure S3 in Supporting Information).

The crystal structure is stabilized by strong N-H···Cl and N-H···O as well as weak C-H···O hydrogen bonds in which the acceptors are the oxygen atoms of perchlorate ions or water molecules. The hydrogen bond geometry data are summarized in Table S3. The packing diagram of the unit cell (Figure S4) indicates the presence of channels filled with perchlorate ions, which are stabilized by weak C-H···O hydrogen bonds.

Hybrid DFT Modelling of the [$Cu_3H_{-4}L_2$] Complex

The trinuclear copper(II) complex can adapt multiple spin states due to various spin coupling schemes among the three $3d^9$ copper(II) sites. A conceptually correct electronic structure description can be calculated for the ferromagnetically coupled (FC) $S_t = 3/2$ state in the collinear spin approximation with each copper(II) sites having an $m_s = +1/2$ spin state. Formally, the spin momentum can be flipped to be $m_s = -1/2$ for one of the copper(II) sites either at the central or one of the peripheral positions. This results in an antiferromagnetically coupled (AFC) $S_t = 1/2$ state, which can be approximated by the broken-symmetry formalism within DFT. In the latter calculation, the result of the computation is a combination of all possible $M_s = 1/2$ levels from the $S_t = 1/2$ and the $S_t = 3/2$ states. Using the expectation value of the spin operator for the $S_t = 3/2$ state and the broken-symmetry $M_s = 1/2$ state, the spin polarized $S_t = 1/2$ energy levels can be estimated.[51]

The optimized structures of [$Cu_3H_{-4}L_2$] complex isolated from its crystal environment are shown in Figure 2 for the antiferromagnetically coupled $M_s = 1/2$ states obtained with different density functionals (the corresponding xyz coordinates are listed in Tables S4 and S5). In both states the optimized structure shows a symmetric environment with respect of the two peripheral ends, which is different than what is seen in the crystal structure. This suggests that there are considerable crystal packing forces that can induce asymmetry between the two ends of the complex. Due to the high symmetry of the calculated structures, we do not differentiate between the two peripheral Cu sites in the computational results.

The calculated Cu spin densities, the spin expectation values, and energy differences between the FC and AFC coupled structures are summarized in Table 3. In all calculations independent of the composition of the hybrid functionals, we found the AFC state to be energetically lower relative to the FC state. The energy difference between the two spin states is greatly dependent on the nature of the density functional. At the most ionic level, the coupling between the sites is negligible since the energy gap between the FC and AFC states is 16 cm^{-1}.

Inclusion of electron correlation in the form of Perdew's 1986 correlation functional increases the gap to 50 cm^{-1}. This increases to close to 2000 cm^{-1} for the pure GGA function, BP86. It is interesting to note that the B3LYP functional gives energy gap about the same as the spectroscopically calibrated B38HFP86 functional despite that it has about the same amount of DF exchange than the B18HFP86 functional. This emphasizes the influence of the nature of the correlation functional in addition to the mixing of HF and DF exchange functionals. The calculated energy gap between the FC and AFC state shown in Table 3 after spin projection can be used to estimate the J coupling value of -4*(ΔE(FC-AFC)) between the two $m_s = \pm 1/2$ sites. For the BS calculations for the AFC state, the central copper(II) site with the tetrapyrazolato coordination environment (formally 2 negative charge) prefers to have m_s = -1/2 spin state, while the peripheral copper(II) ions have m_s = +1/2. As a function of DF exchange vs. HF exchange the energy gap increases from 11 cm^{-1} at HF to 767 cm^{-1} at BP86 level. There was a peculiar switch in the preference of the spin coupling scheme at the B3LYP level where the central copper(II) is preferred to have m_s = +1/2 state while the peripheral has m_s = -1/2 with an unreasonably large energetic preference of 4469 cm^{-1}.

Despite the energetic differences between the FC and AFC states at the B38HFLYP/def2TZVP level there are negligible structural differences for the optimized structures, therefore Figure 2 only shows the lowest energy AFC state in comparison to the B3LYP/def2TZVP structure. However, there are some notable differences between the B3LYP and B38HFLYP structures with the exception of the axial Cu-N interaction at the peripheral sites and the Cu···Cu vectors that are practically identical within a few hundreds of Ångstrøms. Furthermore, negligible differences can be seen in Figure 2 among the angles between the two functionals. This is a stark warning against using only geometric information for evaluation of electronic structure and/or accuracy of the level of theory.

The calculated peripheral and central Cu ion distances are in the range of 3.83–3.89 Å and 3.83–3.94 Å for the FC and AFC states, respectively as a function of the amount of HF exchange in the hybrid density functional. This is about 0.03–0.11 Å longer on average than the experimental value from XRD structure (3.830 Å and 3.767 Å see above). Supporting information (Tables S6 and S7) show that the HF method gives the longest distance, as expected; however, by adding full DF correlation functional, the Cu···Cu distances become the shortest. Gradually adding more DF exchange functional makes this distance elongate to practically the same distance at pure GGA level as in the HF method. The long Cu···Cu distances correlate well with the small coupling constants between the paramagnetic sites (see

above), which indicate that insertion another atom between the two paramagnetic metal sites reduces the strength of the M···L···M super-exchange pathway and pushes the metals far enough to diminish the possibility for M···M direct exchange. The former tend to stabilize the antiferromagnetic state, while the dominance of the latter is responsible for the preference of ferromagnetic state. The Cu-N distances around the central copper(II) ions are in the range of 1.99–2.01 Å for the hybrid functionals and 2.07–2.08 Å at HF level, which clearly highlights the drastic effect of correlation functional. The corresponding bond lengths for the peripheral Cu(II) ions is about 0.1 Å longer with the same differences between DFT and HF calculations as for the central copper(II) ions. This is a reasonable agreement with the experimental Cu(II)-N distances of 1.904-1.973 and 2.014-2.247 Å for the pyrazolato and secondary amino nitrogens, although some of distances are up to 0.05 Å and 0.12 Å longer than experimental values, respectively. The flattened tetrahedral coordination of the central Cu is again reasonably well reproduced with bond angles 94–100º and 137–141º relative to the experimental values of 95.68(15)° and 135.86(15)° at the B38HFP86/def2TZVP level.

The negligible structural differences among the computed structures shown in Figure 2 are in contrast with the calculated atomic spin density distributions in Table 3 where there is about 0.1 *e* difference in the Cu atomic spin densities. As expected, the B3LYP results with less HF exchange are more covalent than the B38HFP86 functional. The large variation in the atomic spin densities between the HF method, the hybrid GGA, and pure GGA functional, while there are insignificant differences among the Cu-N and Cu···Cu distances and N-Cu-N angles, suggest that the covalent interactions do not play a dominant role in the overall chemical bonding and ionic interactions determine the overall structure and thus the complex stability. It is also interesting to note that the central Cu ion has greater spin density than the peripherals in all calculations. This means that the tetrapyrazolato coordination in a flattened tetrahedral arrangements correspond to a less covalent bonding than the peripheral copper(II) ions involved with smaller spin density. This could be rationalized by the difference between the Cu←N(amine) and Cu←N(pyrazolato) charge transfer. The former transfers less electron density to the peripheral Cu ions, which in turn allow for the latter to dominate covalent Cu-N bonding. For the central Cu ion, four strong donors are competing to saturate the electrophilicity of the Cu ion, which results in an overall less covalent bonding and more N…N ligand/ligand repulsion. This electronic structural features may prepare the central copper(II) ion to be the site for catecholate substrate coordination as discussed below.

Solution Chemical Studies

The protonation constants of pyztach are listed in Table 4, together with those of parent tach.[16] Only the amino groups undergo protonation/deprotonation processes in the pH-range of 2-11 studied here. Therefore, the protonation constants of tachpyz are directly comparable with those of tach, indicating notable electron-withdrawing effect of the pyrazole rings.

The interaction of copper(II) with tachpyz was studied at Cu(II)/tachpyz ratios of 1/2, 1/1, 3/2 and 2/1. The combined evaluation of pH-potentiometric and UV-Vis spectrophotometric data indicated the formation of two mononuclear (Cu**H**L, Cu**L**) and three trinuclear ($Cu_3H_{-2}\mathbf{L}_2$, $Cu_3H_{-3}\mathbf{L}_2$ and $Cu_3H_{-4}\mathbf{L}_2$) complexes in the copper(II)-tachpyz system. Their distribution curves are depicted in Figure 3. In equimolar solution, the highly stable Cu**L** complex is the dominant species between pH 4-7. Considering the protonation constants (log β_{0x1}, x = 1, 2, 3) of the free ligand from Table 4, the nearly complete formation of Cu**L** at pH 4 indicates that all the three secondary amines are coordinated. Nevertheless, log β_{101} is more than five orders of magnitude greater than that of the related Cu(tach) complex (Table 4), which suggests additional coordination of 2-3 pyrazole rings. The electronic and EPR spectra were used to the determine the coordination geometry around copper(II) in Cu**L**. The two absorption bands observed on the visible/near IR spectrum of Cu**L** at 634 and 970 nm (Figure 4 and Figure S5 in ESI) clearly indicate square pyramidal geometry around the metal ion with relatively strong apical coordination, similarly to the copper(II) complexes of several related tach derivatives.[25,52] This conclusion is also supported by the EPR parameters related to the species Cu**L** (g_o = 2.1141, A_o = 64.6 G, $g_{x/y/z}$ = 2.040/2.060/2.225, $A_{x/y/z}$ = 20/15/170 G, Figure 5). Consequently, the square pyramidal coordination environment created by three secondary amines and two pyrazole N(1) nitrogens in Cu**L** is similar to the peripheral copper(II) ions in **1**.

Above pH 7 the potentiometric data indicated further deprotonations and the formation of the trinuclear $Cu_3H_{-4}\mathbf{L}_2$ complex. Considering the structure of tachpyz, such processes should involve either copper(II) promoted deprotonations of water molecules or pyrazole N(2)H protons. During the formation of $Cu_3H_{-4}\mathbf{L}_2$ the colour of the solution also changes from blue to reddish, due to the development of intense charge transfer (CT) bands between 400–600 nm (Figure 4). Such CT bands are consistent only with copper(II) promoted deprotonations of pyrazole rings, *i.e.* the formation of pyrazolate-bridged trinuclear core in

$Cu_3H_{-4}\mathbf{L}_2$. Accordingly, beside the identical composition and protonation state, the structure of $Cu_3H_{-4}\mathbf{L}_2$ is also analogous to the crystallographically characterized complex **1**.

At room temperature, the formation of the trinuclear species causes a gradual decrease of the EPR signal intensity between pH 7-10 (Figure 5), due to the antiferromagnetic interaction between the copper(II) centres, mediated by the bridging pyrazolate rings. However, at 77 K a wide singlet (g_{iso} = 2.094, A_{iso} = 25 G) appears in the EPR spectra (that overlaps with the spectrum of the residual Cu**L** species), which is in accordance with a coupled trinuclear core with total spin of S = ½. This is also confirmed by the single-crystal EPR spectra of **1** measured at room temperature, which exhibit a broad quasi-anisotropic signal at g_{iso} ~ 2.1 (Figure S6 in ESI).

The complete transformation of Cu**L** into $Cu_3H_{-4}\mathbf{L}_2$ in equimolar solution is noteworthy, especially considering that its formation results in the liberation of a bound ligand $3Cu\mathbf{L} = Cu_3H_{-4}\mathbf{L}_2 + \mathbf{L} + 4H^+$, despite the high stability of Cu**L**. Therefore, the formation of the trinuclear complex is thermodynamically highly favoured above pH 7, and can be regarded as a pH-driven self-assembly. Since the coordination of copper(II) ion to pyrazole N(1) nitrogens is a pre-requisite for the deprotonation of N(2)H protons at around the neutral pH range, the formation of the trinuclear complex is under the allosteric control of the two terminal copper(II) ions.

The unique charge transfer bands observed between 400–600 nm, related to the pyrazolate-bridged trinuclear core, also appear at metal ion excess ($[Cu^{2+}]/[tachpyz] = 3/2$), however their development is shifted to the lower pH range (pH 4-7, Figure 4) as compared to the equimolar solutions. At copper(II) excess, our pH-potentiometric data support the formation of three trinuclear species with different protonation states, *i.e.* containing different number of pyrazolate-bridges. The individual UV-Vis spectra of these species (Figure S7 in ESI) show continuous intensity increase and blue shift of the CT bands with increasing number of pyrazolate bridges. The complex $Cu_3H_{-2}\mathbf{L}_2$ is always a minor compound between pH 4-6 (Figure 3), the formation of $Cu_3H_{-3}\mathbf{L}_2$ is more pronounced and shows a maximum around pH 5.5, while the already mentioned $Cu_3H_{-4}\mathbf{L}_2$, the aqueous equivalent of the crystallographically characterized complex **1,** becomes the unique species above pH 7. Accordingly, the copper(II) promoted deprotonation of the neutral pyrazole units, *i.e.* the formation of pyrazolate-bridged complexes, starts around pH 4 at 3/2 metal-to-ligand ratio. This is in good agreement with some other pyrazolato-bridged copper(II) complexes.[29]

Kinetic Studies

Since dioxygen activation at ambient conditions is an attractive research goal, a large number of reports on biomimetic models of catechol oxidase appeared in the literature.[28,53] 3,5-di-*tert*-butylcatechol (H_2dtbc, Scheme 2) is a widely used substrate to study catechol oxidase activity of copper(II) complexes,[54-64] since the bulky substituents hinder further oxidation of the product 3,5-di-*tert*-butyl-1,2-benzoquinone (dtbq). Catechol oxidases are type 3 copper enzymes,[65,66] therefore mostly dinuclear complexes[54-61] were used for the biomimetic studies. Nevertheless, several mononuclear[62,63] or trinuclear[64] complexes were also reported to possess notable catecholase activity. Since our aim is to develop redox-active catalysts, we tested the catecholase-like activity of the complexes formed in the copper(II)-tachpyz system.

The oxidation product dtbq has low solubility in water, therefore the kinetic studies were performed in 50% (m/m) ethanol-water solvent mixture. The speciation of the complexes in this medium may somewhat different from those determined in pure aqueous solutions. Our preliminary data indicated that only the trinuclear complexes have measurable catecholase activity. Fortunately, the formation of these complexes can be easily monitored by their characteristic CT bands around 400-600 nm. In 50% (m/m) ethanol-water mixture and at 1.4/1 Cu(II)/tachpyz ratio, the UV-Vis spectra (Figure 6) showed the development of nearly identical CT bands to those determined in aqueous solutions (Figure 4), demonstrating the formation of identical complexes. Difference was found only in the formation of trinuclear complexes being shifted to the lower pH range (see insert in Figure 6), according to the lower polarity of the solvent.

In the cases of catecholase models, the electrochemistry of the complexes have crucial importance, since their reduction potentials should permit the oxidation of catechol derivatives and the subsequent re-oxidation of the reduced copper centers by molecular oxygen to maintain the catalytic cycle. Only irreversible redox couples were present in the cyclic voltammogram of the copper(II)-tachpyz system (see Figure S8 in ESI) recorded in 50% (m/m) ethanol-water solvent mixture with tachpyz/Cu(II) = 1/1.4 ratio at pH 5.6. The relatively well developed reduction peak at E_{pc} = 0.26 V (vs. NHE) indicates notable stabilization of copper(I), and can be tentatively assigned to $Cu^{II}Cu^{II}Cu^{II} \rightarrow Cu^{II}Cu^{I}Cu^{II}$ process, which is followed by two subsequent irreversible reduction steps in the E_{pc} = 0.0 – (-0.7) V range.

The profile of rate constant of H_2dtbc oxidation versus pH at 1.4/1 Cu(II)/tachpyz ratio is distorted bell-shaped curve (Figure 7) with a surprisingly low pH optimum around pH 5.6. This observation suggests the formation of the reactive species between pH 4 and 5.6, then its subsequent transformation into an inactive one at higher pH. This pH – rate constant profile is

not directly comparable with the speciation of the binary complexes, since the oxidation of H_2dtbc promoted by the copper(II) complexes requires the formation of a complex-dtbc ternary adduct. The formation of this adduct is obviously a pH-dependent process, therefore the presence of the strong metal ion binder H_2dtbc may substantially alter the complex formation processes.

In order to obtain some information about the above mentioned ternary species, and on the binding mode of the substrate H_2dtbc, we studied the interaction of 4-nitrocatechol ($H_2$4NC) with the trinuclear complexes. The oxidation of this electron-poor catechol derivative is hindered, and it is a useful chromophoric probe to mimic catechol-metal ion interaction.[67-69] In 50% (m/m) ethanol-water mixture containing $H_2$4NC:tachpyz:Cu(II) in a ratio of 1:2:3, an absorption peak at λ_{max} = 446 nm develops above pH ~ 4 (Figure 8), nearly parallel with the observed catalytic activity for H_2dtbc oxidation (see the insert in Figure 8). The intensity of this band levels off around the pH of the maximum catalytic activity (pH = 5.6). Since the pK_1 of 4-nitrocatechol under this conditions is 7.1 ± 0.1 (this study), at pH 5.6 only a few percent of non-coordinated 4-nitrocatechol are deprotonated. Consequently, the band at 446 nm is related to the copper(II)-bound 4-nitrocatechol, since the interaction of $H_2$4NC with the copper(II) complexes results its deprotonation at considerably lower pH (pK ~ 4.6). The binding mode 4-nitrocatecholate dianion to the trinuclear complexes is not clear. Although, the bidentate η^2 or bridging η^2:η^1 coordination mode to copper(II) complexes exhibits similar CT band at λ_{max} = 440-470 nm,[68,69] the *ca.* 3.8 Å distance between the central and terminal copper(II) ions would allow η^1:η^1 bridging coordination of catechol derivatives, too.[70,71]

The appearance of a plateau around pH 5.6 in the absorbance versus pH profile (Figure 8) indicates that the formation of the ternary complex(es) reached a maximum. The increase of absorbance at 446 nm above pH 6 is due to the deprotonation of the unbound 4-nitrocatechol (λ_{max} of $H4NC^-$ is at 432 nm[67]). Parallel with this process, the oxidation of H_2dtbc promoted by the trinuclear copper(II) complexes diminishes (insert in Figure 8). These observations suggest that the formation of the highly stable $Cu_3H_{-4}\mathbf{L}_2$ species, having a compact coordination sphere around the metal ions, hinders the coordination possibility of the catechol derivatives, which renders the complex unable to promote the oxidation of H_2dtbc.

Since the kinetically active species has a trinuclear core, in principle, more than one catechol derivatives may be coordinated to the metal ions. Therefore, we followed the changes on the UV-Vis spectra at pH 5.7 with increasing concentration of $H_2$4NC (Figure 9).

The absorbances at 446 nm in function of the [$H_2$4NC]/([Cu(II)]/3] ratio (insert in Figure 9) show a breakpoint around one equivalent of 4-nitrocatechol. The experimental data can be well reproduced by assuming the formation of a single ternary species with 1:1 ratio of 4-nitrocatechol and the trinuclear complexes. The calculated apparent association constant for this adduct [($Cu_3H_{-y}L_2$)(4NC)], where y = 2 and 3, is $K_{app} = 4.9\times10^4$ (see the solid line in the insert of Figure 9), which confirms the high coordinating ability of catechol derivatives to the less deprotonated trinuclear core. Under our conditions and at [$H_2$4NC]/([Cu(II)]/3] = 1 *ca*. 54% of 4-nitrocatechol is bound. This is in good agreement with the plateau observed between pH 5.3 and 6 in Figure 8. The increasing absorbance at 446 nm after adding one equivalent of 4-nitrocatechol is related to the completion of adduct formation and to the absorbance of the free 4-nitrocatechol itself. These observations suggest only one strongly bound (4-nitro)catechol to the trinuclear complexes. Fragmentation of the trinuclear complex upon catecholate binding could be also considered, but the loss of catechol oxidase activity above pH 6 suggests that the trinuclear complex remains intact.

In order to have more insights into the mechanism of H_2dtbc oxidation, its rate was measured as a function of the concentration of trinuclear complexes and dioxygen. The rate constants of H_2dtbc oxidation at pH 5.7 show linear dependence on the concentration of dioxygen (Figure 10). Similarly, the reaction shows a first-order dependence on the concentration of trinuclear complexes (Figure 11). The second order rate constant, determined from the plot in Figure 11, is 59.9 M^{-1} s^{-1}, which is indicative of an important catechol oxidase activity of the trinuclear complexes.

The initial rate of the reaction as a function of H_2dtbc concentration (Figure 12) shows saturation kinetics above 30-40 fold excess of substrate over the trinuclear complexes. This indicates a fast pre-equilibrium related to the formation of the catalytically active ternary complex, followed by the rate determining redox processes and the subsequent release of dtbq. The treatment of the data in Figure 12, using the Michaelis-Menten model, yielded the following parameters: k_{cat} = 0.16 s^{-1} and K_M = 1.62 mM. The Michaelis constant (K_M) is in the expected range for di- or trinuclear complexes.[54-61,64,72] On the other hand, the catalytic rate constant (k_{cat}) confirms the high catecholase activity, the trinuclear complexes in 0.05 mM concentration provide c.a. 10^5-fold maximal rate acceleration as compared to the auto-oxidation of H_2dtbc at pH 5.7. Although, there some more active complexes reported in the literature,[60,72] the trinuclear species presented here are unique considering the surprisingly low pH optimum of the catalytic reaction.

The above kinetic data can be interpreted by a simplified mechanism in Scheme 2. Complex $Cu_3H_{-4}\mathbf{L}_2$, the solution equivalent of the crystallographically characterized complex **1**, which is the dominant species at neutral pH, is inactive. Since the doubly deprotonated $Cu_3H_{-2}\mathbf{L}_2$ is only a minor species in aqueous solution, we suggest that the observed catalytic activity is mainly related to the triply deprotonated $Cu_3H_{-3}\mathbf{L}_2$. It forms a stable ternary complex with H_2dtbc in a fast pre-equilibrium, and the catecholate dianion donates electrons to the central and one of the peripheral copper(II) ions to form the product dtbq (in anaerobic conditions a fast stoichiometric redox reaction was observed between the substrate and the trinuclear complexes). Upon product dissociation, the copper(I) centers are re-oxidized by dioxygen. This may happen according to several scenarios,[53] but our experimental data do not allow proposing detailed mechanism. Since the mononuclear Cu**L** species, which has similar coordination environment to the peripheral copper(II) ions in **1**, is not able to promote the oxidation of H_2dtbc, we assume that the central copper(II) ion, with unsaturated coordination sphere, has fundamental role in binding and oxidation of catechols. At higher pH, where four pyrazolato rings are bound to the central copper, the reaction is inhibited, since the substrate is no longer able to coordinate to the trinuclear core.

Conclusions

A new polydentate tripodal ligand with pyrazole-containing legs (**L**×3HCl) has been prepared on the basis of *cis,cis*-1,3,5-triaminocyclohexane, and its interaction with copper(II) was studied. Mononuclear (CuH**L**, Cu**L**) and three trinuclear ($Cu_3H_{-x}\mathbf{L}_2$, x = 2, 3, 4) complexes were identified in solution by combined evaluation of potentiometric, UV-VIS, and EPR data. The mononuclear Cu**L** complex is highly stable, nevertheless it transforms into trinuclear complexes even in equimolar solution. Parallel with the development of trinuclear complexes, intense charge transfer bands appear around 400–500 nm, indicating the formation of pyrazolate-bridged complexes. The crystal structure of $[Cu_3H_{-4}\mathbf{L}_2](ClO_4)_2\times5H_2O$ (**1**) reveals the formation of a unique trinuclear complex that features a tetra(pyrazolate)-bridged linear tricopper(II) core. The two peripheral copper(II) ions have slightly distorted square pyramidal geometry. The four pyrazole rings bound to the two peripheral copper(II) ions are deprotonated and create a Jahn-Teller distorted flattened tetrahedral environment for the central copper(II). Hybrid DFT calculations provided additional details about the geometric and electronic structures of the trinuclear complex showing the preference of the antiferromagnetically coupled ground state with $S_t = 1/2$ ground state. The triply deprotonated

trinuclear complex is an efficient catechol oxidase mimic, which shows a surprisingly low pH optimum around pH = 5.6. Since the mononuclear Cu**L** species is not able to promote the oxidation of 3,5-di-tert-butylcatechol, we assume that the central copper(II) ion with unsaturated coordination sphere has a fundamental role in binding and oxidation of the substrate.

Acknowledgment. This work was supported by the Hungarian Scientific Research Fund (OTKA K101541). RKSz is thankful for the Albert Szent-Györgyi Call-Home Fellowship by the European Union and the State of Hungary, co-financed by the European Social Funds in the framework of TÁMOP 4.2.4.A/2-11-1-2012-0001 'National Excellence Program' and for the computational resources from the National Information Infrastructure Development (NIIF) Program of Hungary. The authors thank Dr. Éva Kováts (Institute for Solid State Physics and Optics, Wigner RCP of the H.A.S.) for the collection of low temperature X-ray diffraction data.

References

[1] Krämer, R.; Gajda, T.; "Functional Model Complexes for Dinuclear Phosphoesterase Enzymes", in *Perspectives on Bioinorganic Chemistry*, ed. R. W. Hay, J. R. Dilwoth and K. Nolan, JAI Press Inc., Stamford, Connecticut, 1999, vol. 4, pp. 207-240.

[2] Williams, N. H.; Takasaki, B.; Wall, M.; Chin, J., *Acc. Chem. Res*., **1999**, *32*, 485.

[3] Molenveld, P.; Engbersen, J. F. J.; Reinhoudt, D. N., *Chem. Soc. Re*v. **2000**, *29*, 75-86.

[4] Gajda, T.; Krämer, R.; Jancsó, A., *Eur. J. Inorg. Chem*. **2000**, 1635

[5] Albedyhl, S.; Schnieders, D.; Jancso, A.; Gajda, T.; Krebs, B., *Eur. J. Inorg. Chem*. **2002**, 1400.

[6]. Gajda, T.; Jancsó, A.; Mikkola, S.; Lönnberg, H.; Sirges, H., *J. Chem. Soc., Dalton Trans.* **2002**, 1757.

[7] Wang, Q.; Leino, E.; Jancsó, A.; Szilágyi, I.; Gajda, T.; Hietamaki, E.; Lönnberg, H., *ChemBioChem* **2008**, *9*, 1739.

[8] Gajda, T.; Düpre, Y.; Török, I.; Harmer, J.; Schweiger, A.; Sander, J.; Kuppert, D.; Hegetschweiler, K., *Inorg. Chem*. **2001**, *40*, 4918.

[9] Jancsó, A.; Mikkola, S.; Lönnberg, H.; Hegetschweiler, K.; Gajda, T., *Chem. Eur. J*., **2003**, *9*, 5404-5415.

[10] Jancsó, A.; Mikkola, S.; Lönnberg, H.; Hegetschweiler, K.; Gajda, T., *J. Inorg. Biochem*., **2005**, *99*, 1283-11293.

[11] Jancsó, A.; Török, I.; Hegetschweiler, K.; Gajda, T.; *ARKIVOC* **2009**, *Part 3*, 217-224.

[12] Cozzi, P. G., *Chem. Soc. Rev*., **2004**, *33*, 410-421

[13] Bryliakov, K. P.; Talsi E. P., *Coord. Chem. Rev.*, **2014**, *276*, 73-96.

[14] Parkin, G., *Chem. Commun*., **2000**, 1971–1985.

[15] Hegetschweiler, K., *Chem. Soc. Rev*., **1999**, *28*, 239-249.

[16] Fujii, Y.; Kiss, T.; Gajda, T.; Tan, X.S.; Sato, T.; Nakano, Y.; Hayashi, Y.; Yashiro, M., *J. Biol. Inorg. Chem*., **2002**, *7*, 843-851.

[17] Itoh, T.; Hisada, H.; Sumiya, T.; Hosono, M.; Usui, Y.; Fujii, Y., *J. Inorg. Biochem*. **1997**, *101*, 348-61.

[18] Sissi, C.; Mancin, F.; Palumbo, M.; Scrimin, P.; Tecilla, P.; Tonellato, U., *Nucleosides Nucleotides Nucleic Acid*s, **2000**, *19*, 1265-71.

[19] Sissi, C.; Mancin, F.; Gatos, M.; Palumbo, M.; Tecilla, P.; Tonellato, U., *Inorg. Chem*. 2**005**, *44*, 2310-2317.

[20] Bollinger, J.E.; Mague, J.T.; Roundhill, D.M., *Inorg. Chem*. **1994**, *33*,1241-2.

[21] Bollinger, J.E.; Mague, J.T.; O'Connor, C.J.; Banks, W.A.; Roundhill, D.M., *J. Chem. Soc*. *Dalton Trans*. **1995**, 1677-88.

[22] Lewis, E.A.; Smith, J.R.L.; Walton, P.H.; Archibald, S.J.; Foxon, S.P.; Giblin, G.M.P., *J. Chem. Soc. Dalton Trans.* **2001**, 1159-1161

[23] Park, G.; Przyborowska, A.M.; Ye, N.; Tsoupas, N.M.; Bauer, C.B.; Broker, G.A.; Rogers, R.D.; Brechbiel, M.W.; Planalp, R.P., *J. Chem. Soc. Dalton Trans.* **2003**, 318.

[24] Park, G.; Lu, F.H.; Ye, N.; Brechbiel, M.W.; Torti, S.V.; Torti, F.M.; Planalp, R.P., *J. Biol. Inorg. Chem.* **1998**, *3*, 449–57.

[25] M.L. Childers, F. Su, A.M. Przyborowska, B. Bishwokarma, G. Park, M.W. Brechbiel, S.V. Torti, F.M. Torti, G. Broker, J.S. Alexander, R.D. Rogers, K. Ruhlandt-Senge, R.P. Planalp, *Eur. J. Inorg. Chem.* **2005**, 3971–3982

[26] Zhao, R.; Planalp, R.P.; Ma, R.; Greene, B.T.; Jones, B.T.; Brechbiel, M.W.; Torti, F.M.; Torti, S.V., *Biochem. Pharm*. **2004**, *67*, 1677-1688.

[27] Klingele, J.; Dechert, S.; Meyer, F.; *Coord. Chem. Rev*. **2009**, *253*, 2698.

[28] Dalle, K.E.; Meyer, F.; *Eur. J. Inorg. Chem.* **2015**, 3391–3405.

[29] Prokofieva, A.; Prikhod'ko, A.I.; Enyedy, E.A.; Farkas, E.; Maringgele, W.; Demeshko, S.; Dechert, S.; Meyer, F.; *Inorg. Chem*. **2007**, *46*, 4298.

[30] Ackermann, J.; Meyer, F.; Kaifer, E.; Pritzkow, H.; *Chem. Eur. J*. **2002**, *8*, 247.
[31] Bowen, T.; Planalp, R.P.; Brechbiel, M.W., *Bioorg. Med. Chem. Lett*. **1996**, *6*, 807–810.
[32] Altomare, A.; Cascarano, G.; Giacovazzo, C.; Guagliardi, A., *J. Appl. Cryst*. **1993**, *26*, 343-350.
[33] Sheldrick, G.M., *Acta Cryst.* **2008**, *A64*, 112-122.
[34] Farrugia, L.J., *J. Appl. Cryst.* **1999**, *32*, 837-838.
[35] Rosotti, F.J.C.; Rosotti, H., The determination of stability constants, McGraw-Hill Book Co., New York, 1962, p. 149.
[36] Högfeldt, E., Stability Constants of Metal-Ion Complexes, Part A. Inorganic Ligands, Pergamon, New York, 1982, p. 32.
[37] Zékány, L.; Nagypál, I.; Peintler, G., PSEQUAD for chemical equilibria, Technical Software Distributors: Baltimore, MD, 1991.
[38] Rockenbauer, A.; Korecz, L., *Appl. Magn. Reson*. **1996**, *10*, 29-43.
[39] Bates, R.G.; Paabo, M.; Robinson, R.A., *J. Phys. Chem*. **1963**, *67*, 1833–1838.
[40] Woolley, E.M.; Hurkot, D.G.; Hepler, L.G., *J. Phys. Chem*. **1970**, *74*, 3908–3913.
[41] Szilagyi, R.K.; Metz, M.; Solomon, E.I., *J. Chem. Phys. A*, **2002**, *106*, 2994-3007.
[42] a) Becke, A. D., *Phys. Rev. A: Gen. Phys*. **1988**, *38*, 3098−3100; b) Perdew, J. P., *Phys. Rev. B: Cond. Mater.* **1986**, *33*, 8822−8824 and erratum *Phys. Rev. B* **1986**, *34*, 7406.
[43] Becke, A. D., *J. Chem. Phys.* **1993**, *98*, 5648−5652.
[44] Szilagyi, R.K.; Solomon, E.I., *J. Am. Chem. Soc.* **2006**, *128*, 15550-15551.
[45] Schäfer, A.; Horn, H.; Ahlrichs, R., *J. Chem. Phys*. **1992**, *97*, 2571–2577; Schäfer, A.; Huber C.; Ahlrichs, R., *J. Chem. Phys*. **1994**, *100*, 5829–5835.
[46] Ryde, U.; Olsson, M. H. M.; Pierloot, K., "The structure and function of blue copper proteins", In *Theoretical Biochemistry. Processes and properties of biological systems*, Eriksson, L.A., ed., Elsevier, Amsterdam, 2001, Theoretical and Computational Chemistry, Vol. 9, 1-56; Siegbahn, P.E.M.; Blomberg, M.R.A., *Chem. Rev*. **2000**, *100*, 421-438.
[47] Szilagyi R.K., Winslow M., J. Comput. Chem. **2006**, *27*, 1385-1397.
[48] Addison, A.W., Rao, T.N., Reedijk, J., van Rijn, J., Verschoor, G.C., *J. Chem. Soc. Dalton Trans.* **1984**, 1349-1356.
[49] Allen, F.H., *Acta Cryst*. **2002**, *B58*, 380-388.
[50] Pal, S.; Barik, A.K.; Gupta, S.; Roy, S.; Mandal, T.N.; Hazra, A.; El Fallah, M.S.; Butcher, R.J.; Peng, S.-M.; Lee, G.-H.; Kar, S.K.; *Polyhedron* **2008**, *27*, 357–365.
[51] Clark, A. E.; Davidson, E. R. *J. Chem. Phys.* **2001**, *115*, 7382– 7392.
[52] G. Park, J. Shao, F.H. Lu, R.D. Rogers,N.D. Chasteen,M.W. Brechbiel, R.P. Planalp, *Inorg. Chem.* **2001,** *40*, 4167-4175; G. Park, E. Dadachova, A. Przyborowska, S.-j. Lai, D. Ma, G. Broker, R.D. Rogers, R.P. Planalp, M.W. Brechbiel, *Polyhedron* 20 (2001) 3155–3163
[53] Koval, I.A.; Gamez, P.; Belle, C.; Selmeczi, K.; Reedijk, J.; *Chem. Soc. Rev*., **2006**, *35*, 814–840
[54] Reim, J.; Krebs, B.; *J. Chem. Soc. Dalton Trans*. **1997**, 3793.
[55] Gentschev, P.; Möller, N.; Krebs, B.; *Inorg. Chim. Acta*, **2000**, *300-302*, 442.
[56] Fernandes, C.; Neves, A.; Bortoluzzi, A.J.; Mangrich, A.S.; Rentschler, E.; Szpoganicz, B.; Schwingel, E., *Inorg. Chim. Acta*, **2001**, **320**, 12.
[57] Neves, A.; Rossi, L.M.; Bortoluzzi, A.J.; Szpoganicz, B.; Wiezbicki, C.; Schwingel, E.; Haase, W.; Ostrovsky, S., *Inorg. Chem*. **2002**, *41*, 1788.
[58] Belle, C.; Beguin, C.; Gautier-Luneau, I.; Hamman, S.; Philouze, C.; Pierre, J.L.; Thomas, F.; Torelli, S., *Inorg. Chem*. **2002**, *41*, 479-491.
[59] Granata, A.; Monzani, E.; Casella, L., *J. Biol. Inorg. Chem*. **2004**, *9*, 903–913.
[60] Ackermann, J.; Buchler, S.; Meyer, F., *C. R. Chimie* **2007**, *10*, 421-432.

[61] Selmeczi, K.; Réglier, M.; Giorgi, M.; Speier, G., *Coord. Chem. Rev*. **2003**, *245*, 191–201.
[62] Kaizer, J.; Pap, J.; Speier, G.; Párkányi, L.; Korecz, L.; Rockenbauer, A.; *J. Inorg. Biochem.* **2002**, *91*, 190.
[63] Malachowski, M.R.; Carden, J.; Davidson, M.G.; Driessen, W.L.; Reedijk, J., *Inorg. Chim. Acta* **1997**, *257*, 59.
[64] Das, L.K.; Biswas, A.; Kinyon, J.S.; Dalal, N.S.; Zhou, H.; Ghosh, A., *Inorg. Chem.* **2013**, *52*, 11744–11757
[65] Klabunde, T.; Eicken, C.; Sachettini, J.C.; Krebs, B., *Nat. Struct. Biol*. **1998**. *5*, 1084.
[66] Hakulinen, N.; Gasparetti, C.; Kaljunen, H.; Kruus, K.; Rouvinen, J.; *J. Biol. Inorg. Chem.* **2013**, *18*, 917–929.
[67] Tyson, C.A., *J. Biol. Chem*. **1975**, *250*, 1765.
[68] Plenge, T.; Dillinger, R.; Santagostini, L.; Casella, L.; Tuczek, F., *Z. Anorg. Allg. Chem.* **2003**, *629*, 2258-2265
[69] Kaizer, J.; Zsigmond, Z.; Ganszky, I.; Speier, G.; Giorgi, M.; Réglier, M., *Inorg. Chem.* **2007**, *46*, 4660-4666.
[70] Karlin, K.D.; Gultneh, Y.; Nicholson, T.; Zubieta, J., *Inorg. Chem*. **1985**, *24*, 3725–3727.
[71] Borzel, H.; Comba, P.;, Pritzkow, H., *Chem. Commun*. **2001**, 97–98
[72] J. Mukherjee, R. Mukherjee, Inorg. Chim. Acta, 2002, 337, 429–438

Table 1. Crystallographic data for the complex $[Cu_3H_{-4}\mathbf{L}_2](ClO_4)_2\times 5H_2O$ (**1**)

Crystal data	
Chemical formula	$C_{36}H_{50}Cu_3N_{18}\cdot 2(ClO_4)\cdot 4(H_2O)\cdot O$
M_r	1212.52
Crystal system, space group	Monoclinic, $P2_1/c$
Temperature (K)	100
a, b, c (Å)	13.0393 (2), 28.5503 (4), 13.3878 (2)
β (°)	105.004 (2)
V (Å^3)	4814.04 (13)
Z	4
μ (mm^{-1})	3.26
Crystal size (mm)	0.4 × 0.06 × 0.02
Data collection	
Absorption correction	Multi-scan
T_{min}, T_{max}	0.720, 1.000
No. of measured, independent and observed [$I > 2\sigma(I)$] reflections	35344, 9485, 8187
R_{int}	0.029
$(\sin\theta/\lambda)_{max}$ (Å^{-1})	0.622
Refinement	
$R[F^2 > 2\sigma(F^2)]$, $wR(F^2)$, S	0.074, 0.225, 1.04
No. of reflections, parameters, restraints	9485, 681, 123
H-atom treatment	H-atom parameters constrained
$\Delta\rangle_{max}$, $\Delta\rangle_{min}$ (e Å^{-3})	1.48, -1.38

Table 2. Selected interatomic distances (Å) and angles (◦) of the complex $[Cu_3H_{-4}\mathbf{L}_2](ClO_4)_2\times 5H_2O$ (**1**)

N1-Cu1	2.219(4)	N1-Cu1-N2	93.9(2)
N2-Cu1	2.049(4)	N1-Cu1-N3	93.7(2)
N3-Cu1	2.031(4)	N1-Cu1-N22	101.2(2)
N22-Cu1	1.936(4)	N1-Cu1-N32	106.9(2)
N32-Cu1	1.954(4)	N2-Cu1-N3	90.5(2)
N21-Cu2	1.962(4)	N2-Cu1-N22	82.8(2)
N31-Cu2	1.971(4)	N2-Cu1-N32	158.4(2)
N71-Cu2	1.973(4)	N3-Cu1-N22	164.0(2)
N81-Cu2	1.960(4)	N3-Cu1-N32	82.7(2)
N51-Cu3	2.262(4)	N22-Cu1-N32	98.3(2)
N52-Cu3	2.041(4)	N21-Cu2-N31	100.5(2)
N53-Cu3	2.040(4)	N21-Cu2-N71	96.7(2)
N72-Cu3	1.946(4)	N21-Cu2-N81	136.5(2)
N82-Cu3	1.931(4)	N31-Cu2-N71	130.9(2)
		N31-Cu2-N81	95.7(2)
		N71-Cu2-N81	102.6(2)
		N51-Cu3-N52	90.4(2)
		N51-Cu3-N53	93.5(2)
		N51-Cu3-N72	103.7(2)
		N51-Cu3-N82	102.8(2)
		N52-Cu3-N53	93.4(2)
		N52-Cu3-N72	82.0(2)
		N52-Cu3-N82	166.3(2)
		N53-Cu3-N72	162.1(2)
		N53-Cu3-N82	82.2(2)
		N72-Cu3-N82	98.2(2)

Table 3. Summary of electronic structural results (<S^2> expectation value of spin operator, MPA = Mulliken Population Analysis in electrons, ΔE is for spin projected pure AFC state), relative energies between the ferromagnetic (FC) and antiferromagnetic (AFC) states (coupling scheme indicates the orientation of the spin moments with α and β corresponding to m_s = +1/2 and -1/2) using various DFT functionals and def2TZVP basis set.

	ferromagnetic S^t = 3/2 state				antiferromagnetic M_s = 1/2 state				
		MPA		ΔE(FC-AFC)	Coupling		MPA		ΔE(ααβ−αβα)
Functional	<S^2>	Cu^c	Cu^p	cm^{-1}	Scheme	<S^2>	Cu^c	Cu^p	cm^{-1}
HF	3.7630	0.92	0.87	16	ααβ	1.7621	0.92	-0.87	11
					αβα	1.7612	-0.92	0.87	0
HFP86	3.7619	0.89	0.84	50	ααβ	1.7627	0.89	-0.84	28
					αβα	1.7611	-0.89	0.84	0
B75HFP86	3.7613	0.86	0.79	91	ααβ	1.7608	0.85	-0.79	46
					αβα	1.7602	-0.85	0.79	0
B38HFP86	3.7602	0.74	0.66	307	ααβ	1.7557	0.73	-0.66	152
					αβα	1.7513	-0.73	0.66	0
B3LYP	3.7577	0.64	0.58	308	ααβ	1.7394	0.63	-0.57	0
					αβα	1.7196	-0.64	0.58	4469
B18HFP86	3.7575	0.63	0.57	1296	ααβ	1.7380	0.64	-0.58	264
					αβα	1.7209	-0.63	0.58	0
BP86	3.7540	0.53	0.49	1946	ααβ	1.4998	0.47	-0.41	767
					αβα	1.3792	-0.43	0.43	0

Table 4. Logarithmic formation constants of the proton and copper(II) complexes of tachpyz and tach (*T* = 298 K, I=0.1M (NaCl), with estimated errors in parentheses (last digit)).

pqr	log β_{pqr}	
	tachpyz	tach[a]
031	21.50(1)	25.93
021	16.00(1)	18.88
011	8.84(1)	10.21
111	18.80(5)	15.95
101	16.10(3)	10.86
1-11	-	2.36
2-22	-	8.48
3-22	27.97(10)	-
3-32	23.11(7)	-
3-42	17.25(8)	-

[a] ref. [16] *I* = 0.1 M $NaClO_4$

Legends

Scheme 1. Schematic structure of tachpyz (L)

Scheme 2. Simplified mechanism of the oxidation of H_2dtbc

Figure 1. PLUTO view of the trinuclear complex **1** with partial numbering scheme. Perchlorate counter ions, water molecules as well as hydrogen atoms were omitted for clarity

Figure 2. Optimized structures of the antiferromagnetically coupled M_s = 1/2 states of $[Cu_3H_{-4}\mathbf{L}_2]$ complex at the B38HFP86/def2TZVP level (αβα coupling, panel A) and at the B3LYP/def2TZVP level (ααβ coupling, panel B) with selected distances in Å and angles in degrees (H atoms are omitted for clarity).

Figure 3. Speciation diagram of the copper(II)-tachpyz 1:1 (A) and 3:2 (B) systems (T = 298 K, I = 0.1 M NaCl, $[Cu^{2+}]$ = 0.001 M (A), 0.003 M (B)).

Figure 4. Effect of pH on the UV-VIS spectra of the copper(II)-tachpyz 1:1 (A) and 3:2 (B) systems **(**T = 298 K, I = 0.1 M NaCl, $[Cu^{2+}]$ = 0.00191 M). The inserts show the changes of absorbances at 508 nm (filled square), 660 nm (open square) and 800 nm (triangle).

Figure 5. Experimental (red) and simulated (black) EPR spectra of the copper(II)-tachpyz systems at room temperature (A) and at 77 K (B). The calculated anisotropic spectra of the two main species (CuL and $Cu_3H_{-4}\mathbf{L}_2$) are also shown in B.

Figure 6. Effect of pH on the UV-VIS spectra of the copper(II)-tachpyz 3:2 system in 50 w% ethanol-water **(**T = 298 K, I = 0.1 M NaCl, $[Cu^{2+}]$ = 0.00198 M). The insert compares the changes of absorbances at 500 nm in 50 w% ethanol-water (filled square) and in pure water (open square, see Figure 4).

Figure 7. pH–rate constant profile of the oxidation of H_2dtbc in 50 w% ethanol-water promoted by the copper(II)-tachpyz 3:2 system (T = 298 K, $[Cu^{2+}]/3$ = 0.05 mM, $[H_2dtbc]_0$ = 1.8 mM).

Figure 8. pH dependent UV-Vis spectra of the $H_2$4NC:tachpyz:Cu(II) = 1:2:3 system in 50 w% ethanol-water mixture. The insert shows the change of absorbance at 446 nm together with the pH-rate constant profile from Figure 7 ($[Cu^{2+}]$ = 0.289 mM, $[H_2$4NC] = 0.096 mM).

Figure 9. UV-Vis spectra of the Cu(II)/tachpyz 3/2 system in 50 w% ethanole-water solution titrated by 0 – 8 equivalents of $H_2$4NC, insert shows the change of absorbance at 450 nm as a function of the $[H_2$4NC]/([Cu(II)]/3] ratio, dashed line indicate the spectra of 0.5, 1.0 and 2.0 equivalents of 4-nitrocatechole alone ($[Cu^{2+}]/3$ = 0.05 mM, pH = 5.7).

Figure 10. The dependence of the rate constant of H_2dtbc oxidation on the complex concentration ($[Cu^{2+}]$/[tachpyz] = 3/2, pH = 5.7, $[H_2dtbc]_0$ = 1.8 mM).

Figure 11. The dependence of the rate constant of H_2dtbc oxidation catalyzed by the Cu(II)/tachpyz 3/2 system on the dioxygen concentration ($[Cu^{2+}]/3$ = 0.05 mM, pH = 5.7, $[H_2dtbc]_0$ = 1.8 mM).

Figure 12. The dependence of the reaction rate of the aerobic oxidation of H_2dtbc catalyzed by the Cu(II)/tachpyz 3/2 system on the H_2dtbc concentration ([Cu^{2+}]/3 = 0.05 mM, pH = 5.7).

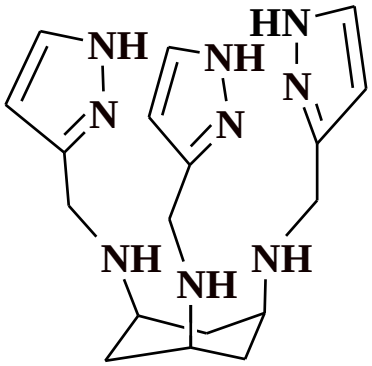

Scheme 1

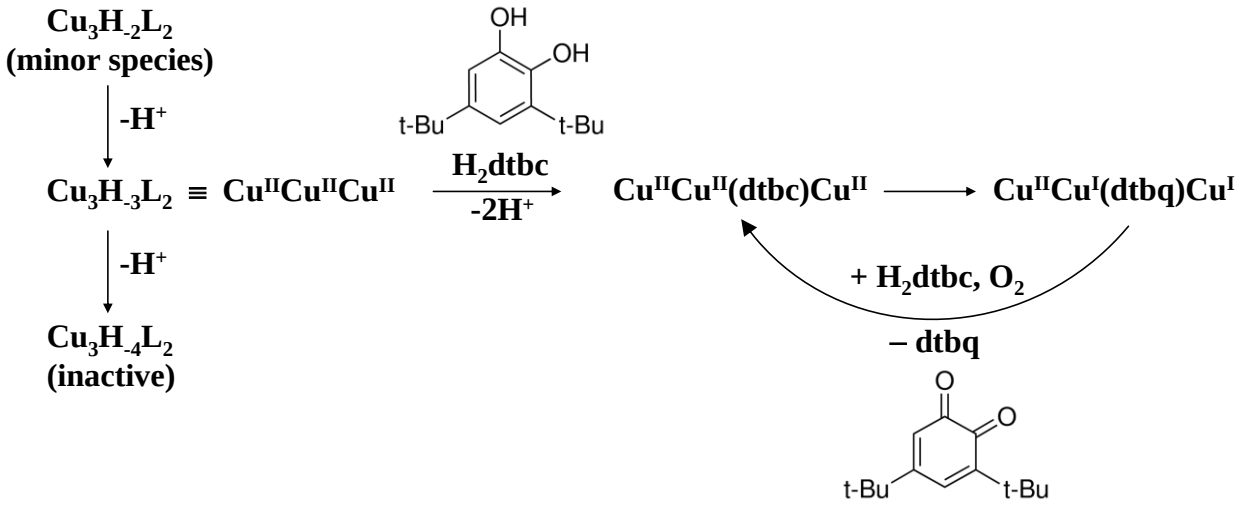

Scheme 2

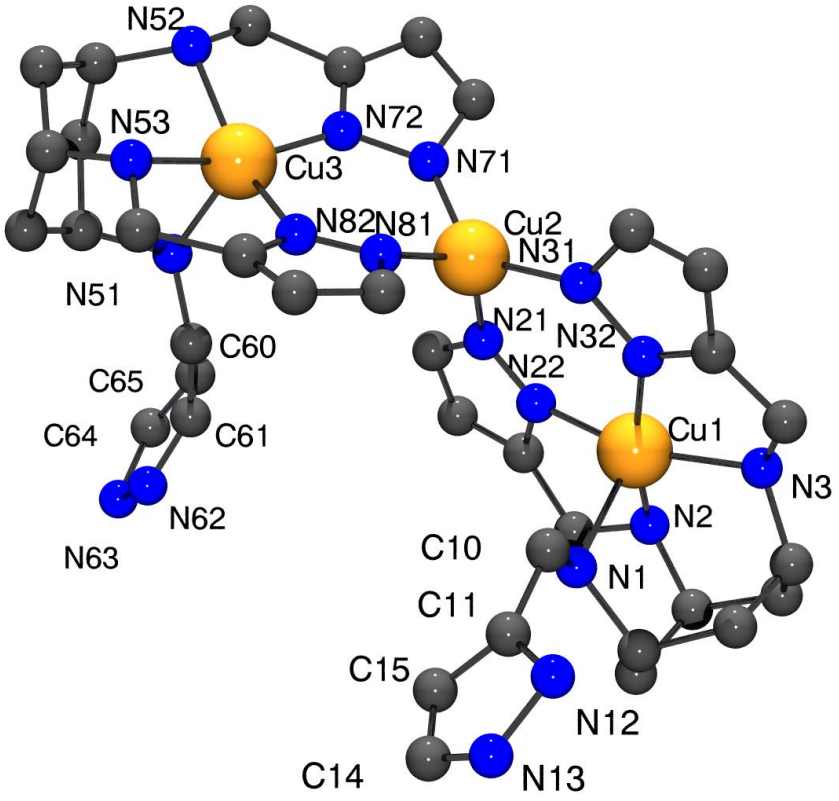
N52
N53
N72
Cu3
N71
N82
N81
Cu2
N31
N51
N21
N32
C60
N22
C65
C64
C61
Cu1
N3
N62
N2
N63
C10
N1
C11
C15
N12
C14
N13

Figure 1

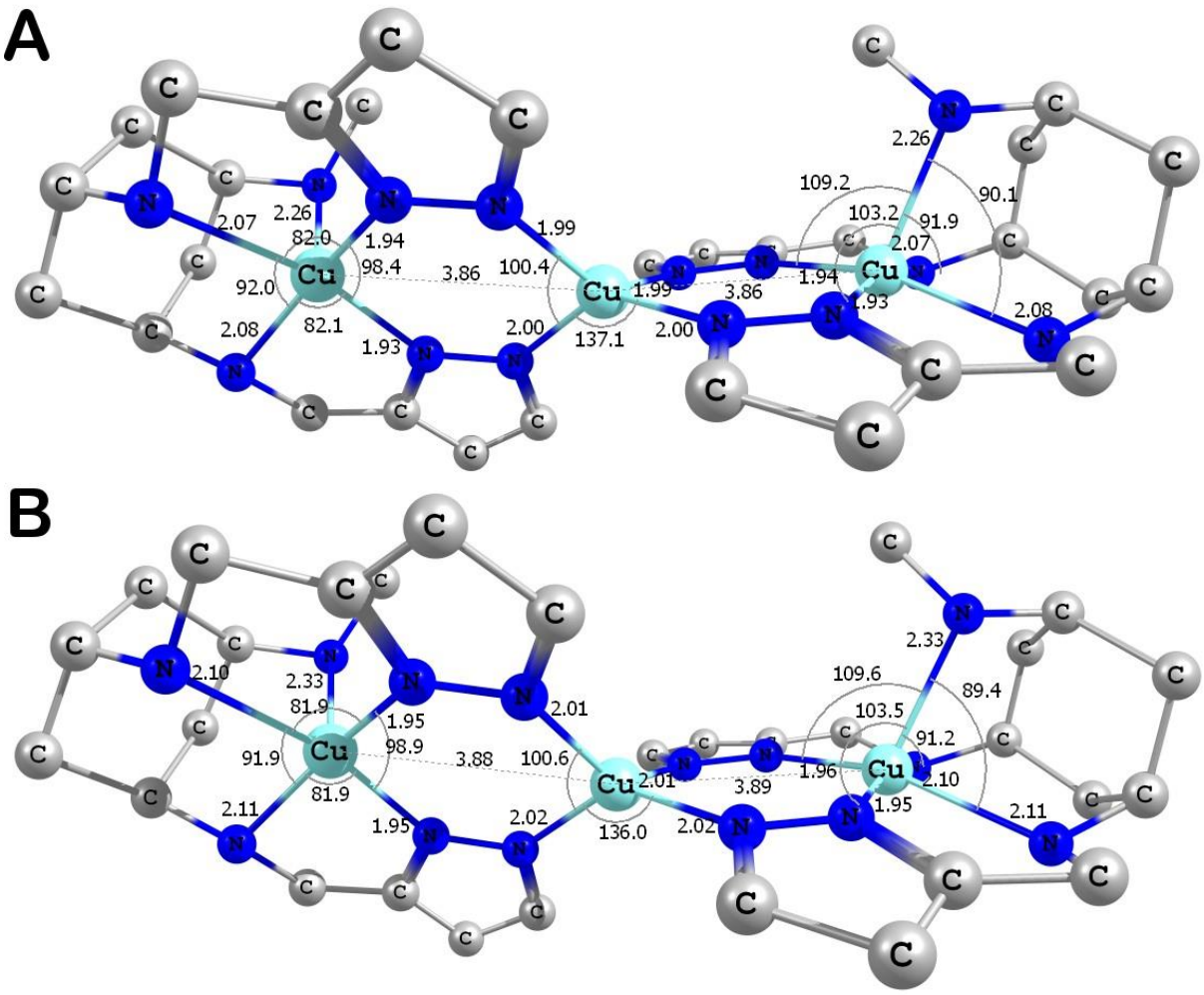

Figure 2.

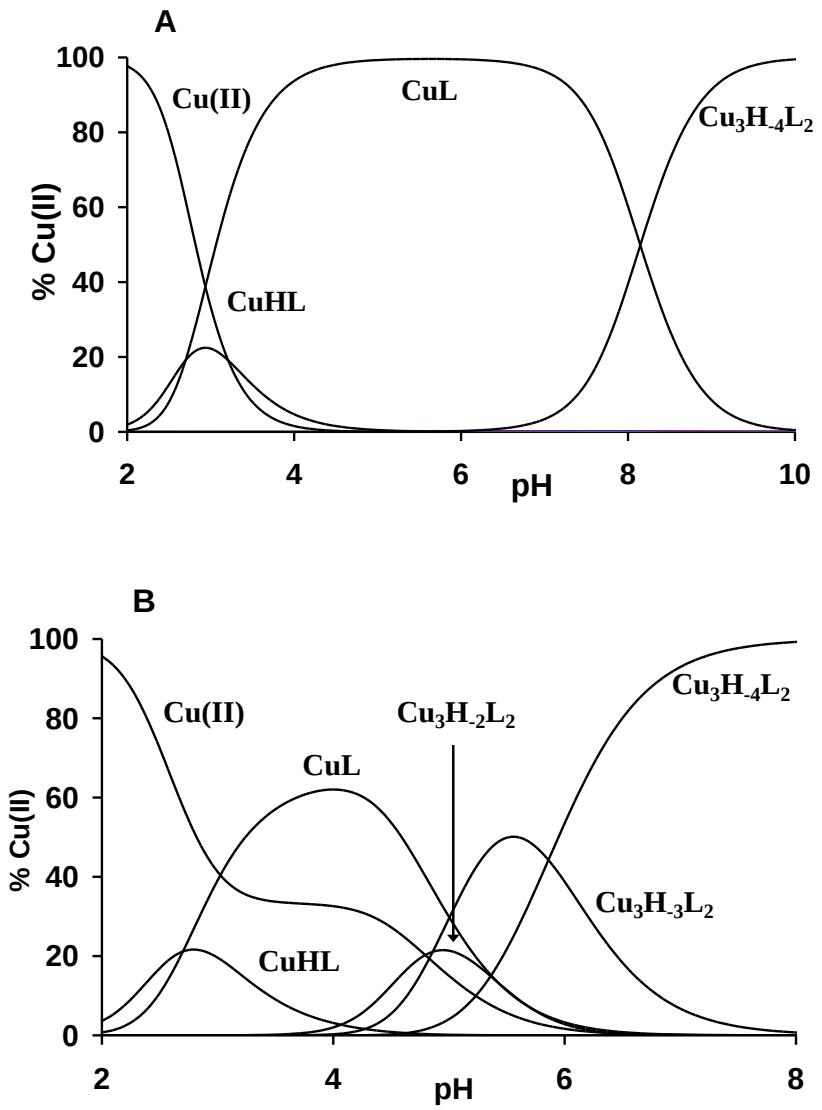
A
100
80
60
40
20
0
% Cu(II)
Cu(II)
CuL
Cu3H-4L2
CuHL
2
4
6
8
10
pH
B
100
80
60
40
20
0
% Cu(II)
Cu(II)
Cu3H-2L2
Cu3H-4L2
CuL
Cu3H-3L2
CuHL
2
4
6
8
pH

Figure 3

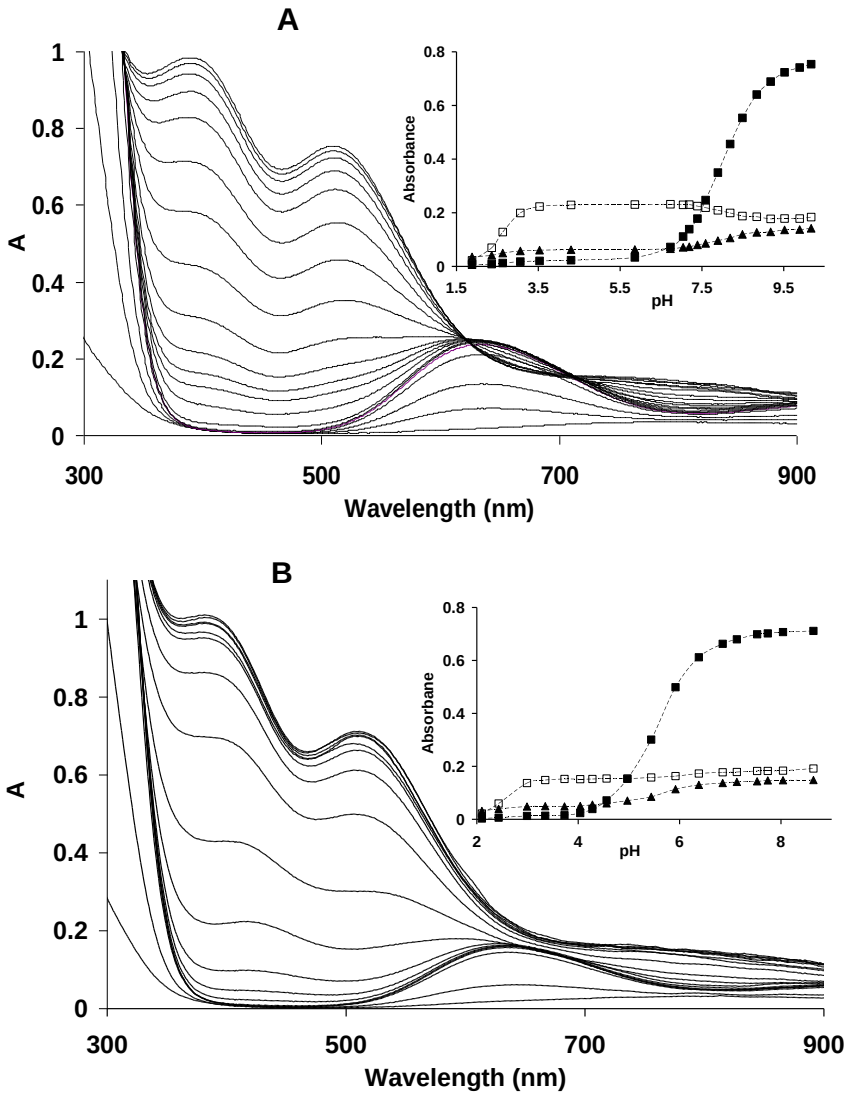
A
A
Wavelength (nm)
Absorbance
pH
B
A
Wavelength (nm)
Absorbane
pH

Figure 4

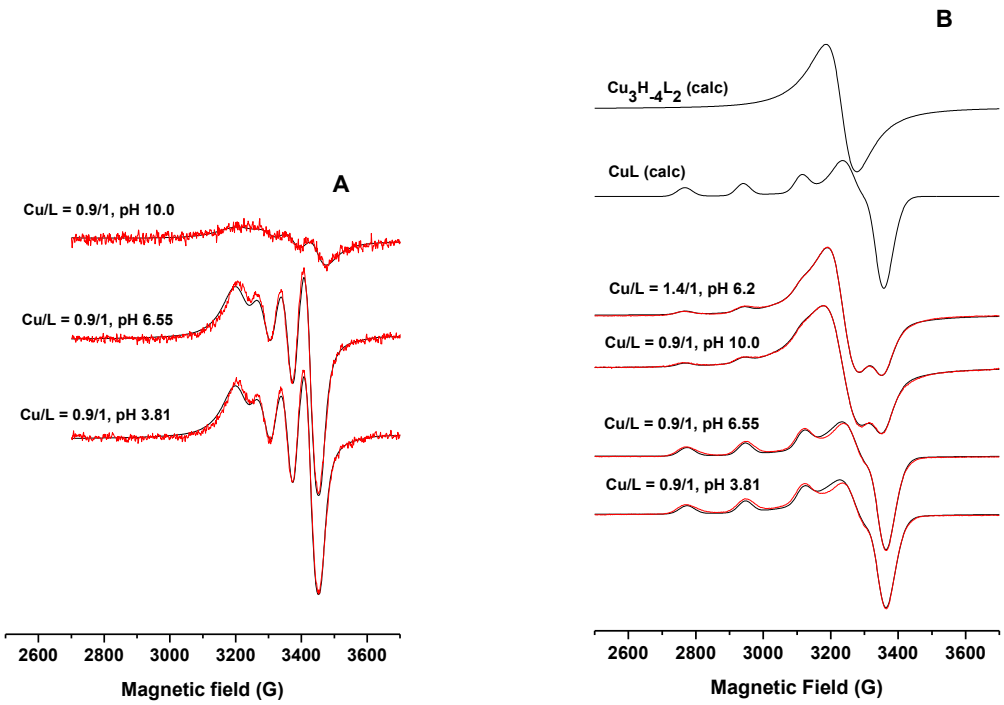
A
Cu/L = 0.9/1, pH 10.0
Cu/L = 0.9/1, pH 6.55
Cu/L = 0.9/1, pH 3.81
2600
2800
3000
3200
3400
3600
Magnetic field (G)
B
Cu3H-4L2 (calc)
CuL (calc)
Cu/L = 1.4/1, pH 6.2
Cu/L = 0.9/1, pH 10.0
Cu/L = 0.9/1, pH 6.55
Cu/L = 0.9/1, pH 3.81
2600
2800
3000
3200
3400
3600
Magnetic Field (G)

Figure 5

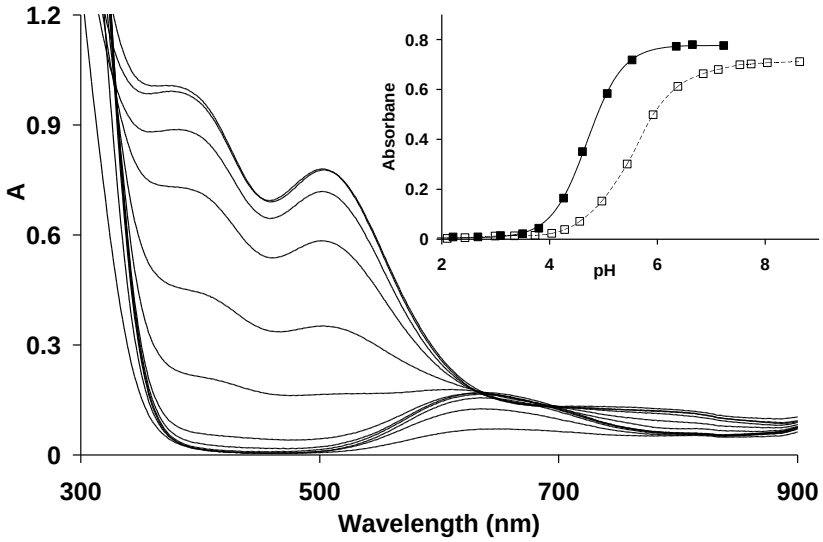
1.2
0.9
0.6
0.3
0
A
300
500
700
900
Wavelength (nm)
0.8
0.6
0.4
0.2
0
Absorbane
2
4
6
8
pH

Figure 6.

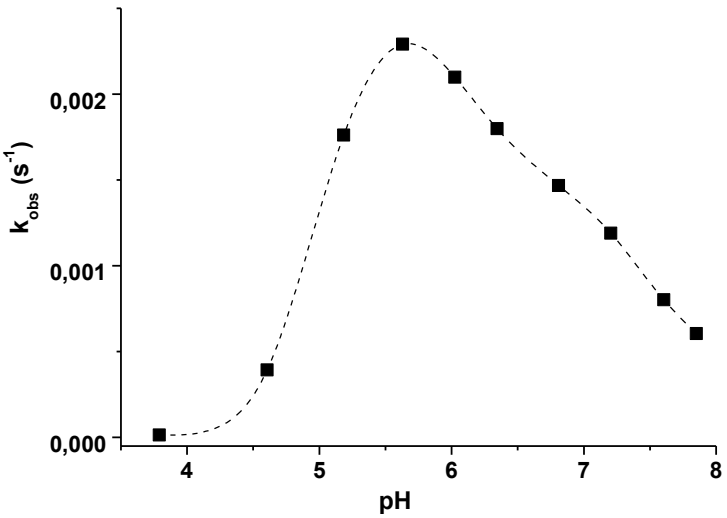

Figure 7.

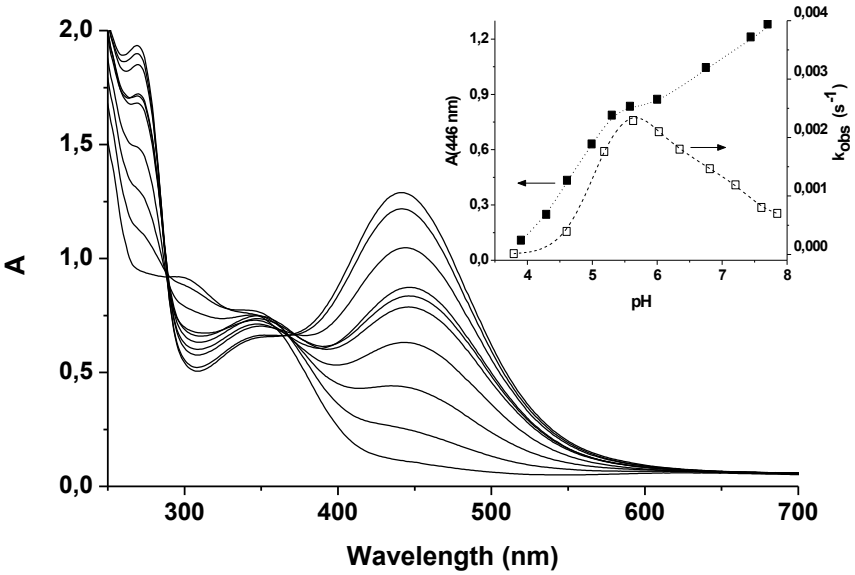

Figure 8.

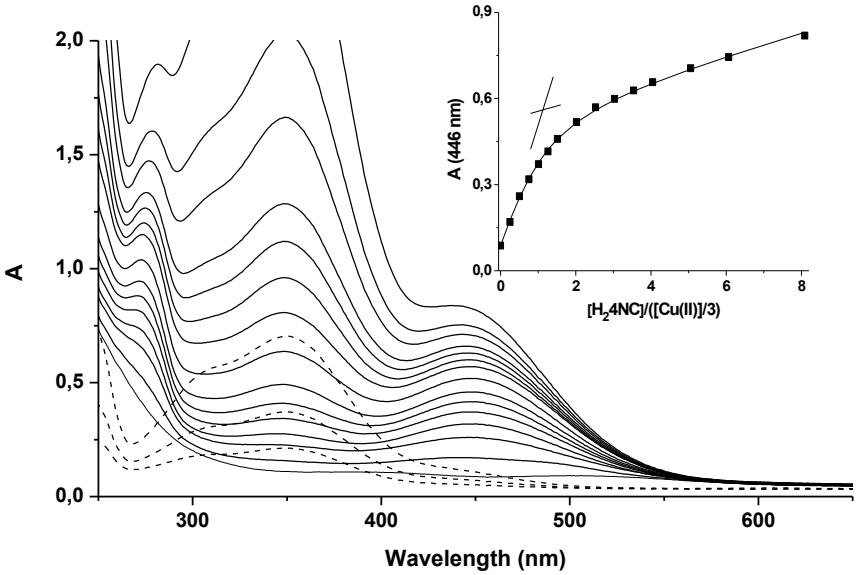

Figure 9.

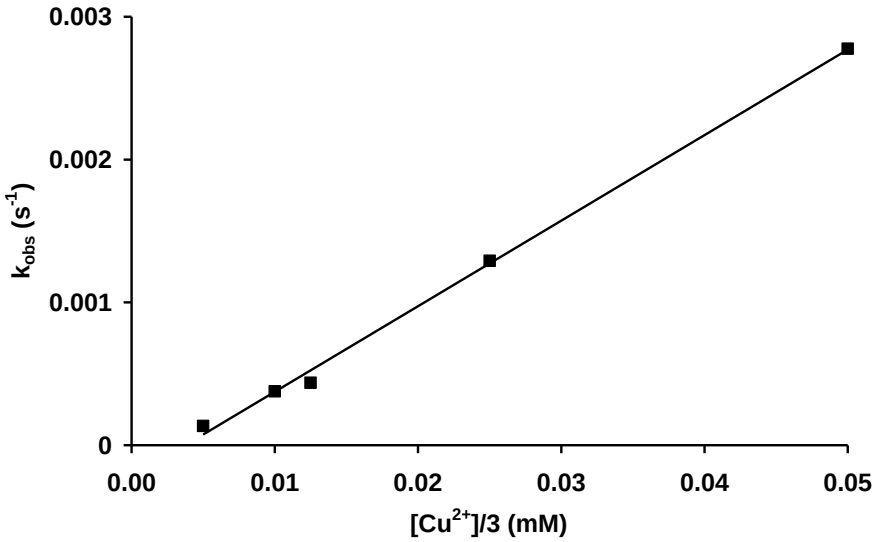

Figure 10.

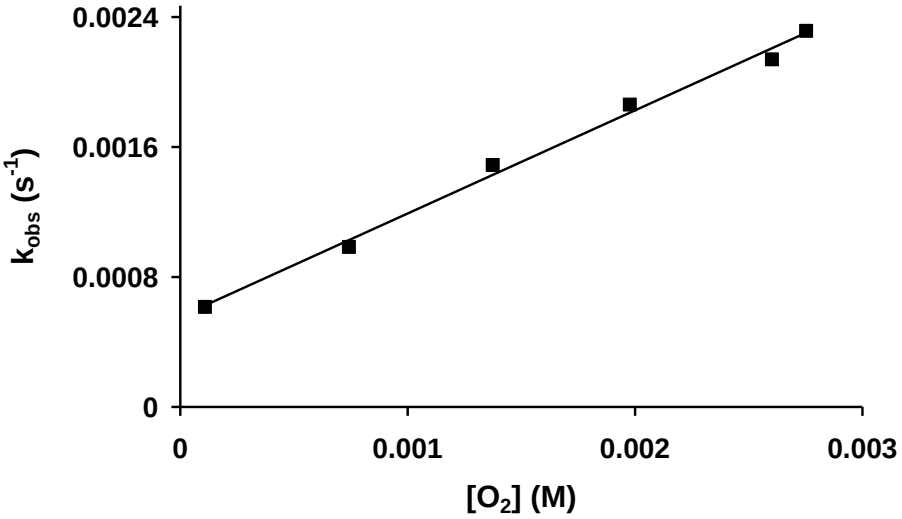

Figure 11.

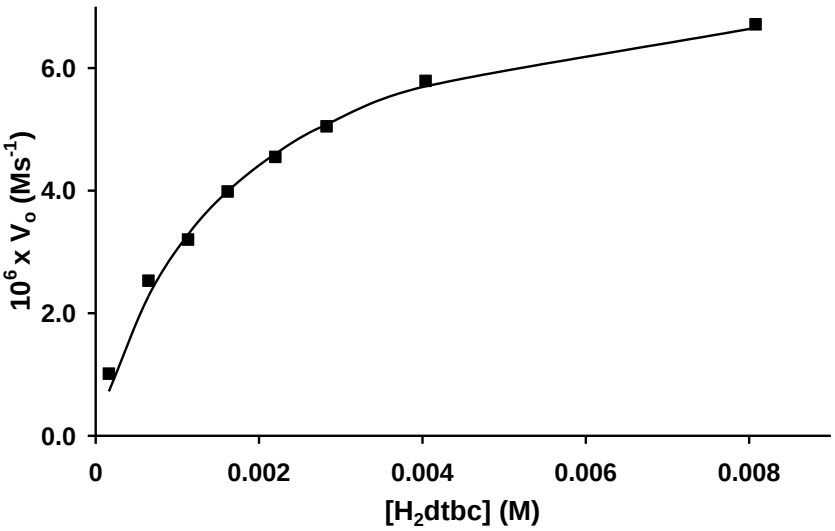

Figure 12.

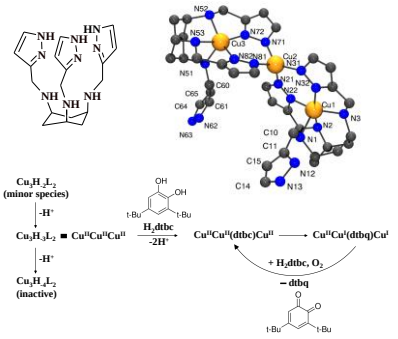

A polydentate tripodal ligand forms a series of trinuclear complexes with copper(II), that feature unique di-, tri-, and tetra(pyrazolate)-bridged linear tricopper(II) core. The triply deprotonated trinuclear complex is a highly efficient catechol oxidase mimic with a surprisingly low pH optimum at pH = 5.6.